IEEE Photonics Journal
An IEEE Photonics Society Publication

Open Access

UV Adhesive Diaphragm-Based FPI Sensor for Very-Low-Frequency Acoustic Sensing

Volume 8, Number 1, February 2016

Li Liu
Ping Lu
Shun Wang
Xin Fu
Yuan Sun
Deming Liu
Jiangshan Zhang
Hao Xu
Qiuping Yao

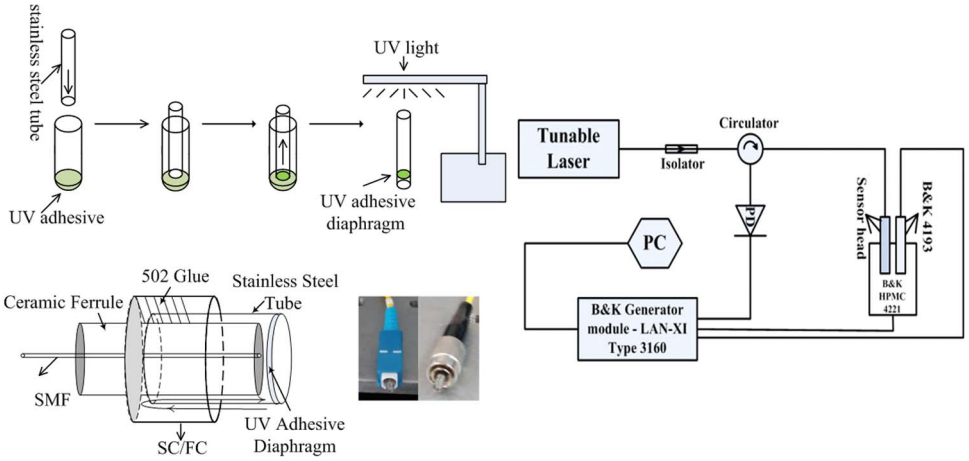

DOI: 10.1109/JPHOT.2015.2509866

IEEE photonics SOCIETY

IEEE

UV Adhesive Diaphragm-Based FPI Sensor for Very-Low-Frequency Acoustic Sensing

Li Liu,[1] Ping Lu,[1] Shun Wang,[1] Xin Fu,[1] Yuan Sun,[1] Deming Liu,[1] Jiangshan Zhang,[2] Hao Xu,[3] and Qiuping Yao[3]

[1]Wuhan National Laboratory for Optoelectronics, National Engineering Laboratory for Next Generation Internet Access System, School of Optical and Electronic Information, Huazhong University of Science and Technology, Wuhan 430074, China
[2]Department of Electronics and Information Engineering, Huazhong University of Science and Technology, Wuhan 430074, China
[3]Hubei Provincial Institute of Measurement and Testing, National Optical Products Inspection Services Center, Wuhan 430071, China

DOI: 10.1109/JPHOT.2015.2509866

Manuscript received November 9, 2015; revised December 9, 2015; accepted December 11, 2015. Date of publication December 17, 2015; date of current version December 30, 2015. This work was supported by the National Natural Science Foundation of China under Grant 61275083 and Grant 61290315 and in part by a grant from the Fundamental Research Funds for the Central Universities.
Corresponding author: P. Lu (e-mail: pluriver@mail.hust.edu.cn).

Abstract: In this paper, we propose and demonstrate a fiber-optic extrinsic Fabry–Pérot interferometer (FPI) sensor based on an ultraviolet (UV) adhesive diaphragm for very-low-frequency acoustic sensing. The sensing diaphragm is formed by the surface tension of UV adhesive solution and exhibits a good acoustic response from 1 Hz to 20 kHz. The sensor has a sensitivity of 57.3 mV/Pa at 1000 Hz and a flat frequency response ranging from 1 to 2000 Hz with a small fluctuation of about ±1.5 dB. The good response of infrasound and rather simple fabrication process make it a wonderful candidate for very-low-frequency acoustic sensing.

Index Terms: Fabry–Pérot interferometer (FPI), ultraviolet (UV) adhesive diaphragm, very-low-frequency, acoustic sensing.

1. Introduction

Very-low-frequency acoustic sensors have been studied extensively for decades and used widely. Infrasound is a new horizon for the remote sensing of the Earth's atmospheric physical environment, and many previous reports have pointed out the existence of infrasound waves generated by many environmental such as sources, volcanic eruptions, ocean waves, earthquakes [1]. Besides, infrasound sensing has been used to detect nuclear explosion in military field [2]. Pipeline leakage detection [3] and medical treatment [4] are also the significant applications of infrasound detection. Due to the good dynamic performance, high sensitivity and signal-to-noise ratio (SNR), the capacitive or piezoelectric acoustic sensors such as MB2000 (France), B&K 4193 and 4964 are the main commercial products for low frequency measurement. Nevertheless, containing many electronic components and electric cable, they are not immune to electromagnetic interference and less practical in the application of long distance.

For the unique advantages of high sensitivity, immunity to electromagnetic interference (EMI), remote detection and multiplexing capability [5], fiber optic acoustic sensors can remove these limitations. Fiber Bragg gratings (FBGs), the Mach-Zehnder interferometer (MZI)/Michelson

interferometer (MI), and the Fabry–Pérot interferometer (FPI) are three major configurations for acoustic detection [6]. FBGs can be modulated by the acoustic wave which wavelength is smaller than the FBG length, but they are insensitive to the low-frequency acoustic wave [7]. MZI/MI based acoustic sensors are the most cost-effective and easy to implement. Zumberge has proposed a MZI structure with two arms wrapped on a very long sealed tube (89 m length and 25 mm diameter silicon rubber) to detect infrasound signal around 1–10 Hz [8]. Even though the size of the MZI/MI sensing head can be reduced by using tapered or hollow-core fibers, the size is still larger [9], [10]. FPI-based acoustic sensors which formed between a cleaved fiber end and a reflective diaphragm are the most sensitive fiber-optic acoustic sensors reported so far and now starting to compete with the standard used piezoelectric transducer (PZT) sensors in terms of the frequency range, resolution, and sensitivity [6]. In the last decades, various kinds of diaphragm materials have been studied for FPI pressure or acoustic sensors, such as silicon [11], polymer [12], graphene [13], chitosan [14], and silver [15]. Moreover, the sensitivity of FPI acoustic sensors can be remarkably improved by reducing thickness-to-diameter ratio of diaphragm [11], [12]. However, the production process of diaphragms such as polymer-based film [16], metal-based film [15], micro-machined silicon diaphragm [17], or single/multi-mode fiber diaphragm [18] is complex and costly, which involves mechanical spinning, chemical etching, or micro-machining. Besides, most of FPI-based acoustic sensors haven't been designed to detect very-low-frequency acoustic wave [11]–[15].

In this paper, an UV adhesive diaphragm based sensor is proposed to offer high sensitivity, good low frequency response, low-cost and easy fabrication for the very low frequency acoustic measurement. The UV adhesive diaphragm with a radius of 1 mm and a thickness of 2.2~6.4 μm is formed by the surface tension of UV adhesive solution. Moreover, UV adhesive can be completely solidified under the ultraviolet light and still keep flexibility, reflective and stability after solidifying. Due to the lower thickness-to-diameter ratio and larger elasticity of UV adhesive diaphragm, the proposed sensor presents a preponderance to detect very-low-frequency acoustic wave with a sensitivity of 57.3 mV/Pa at 1000 Hz and a flat frequency response ranging from 1 Hz to 2000 Hz with a small fluctuation about ±1.5 dB.

2. Working Principle and Sensor Fabrication

When the acoustic pressure is applied to the diaphragm, this imposed pressure will cause the deformation of diaphragm and result in change of the cavity length d. In our experiment, only the center deflection of diaphragm is of interest. For a rigidly clamped round diaphragm, the center deformation is given by [19]

$$\Delta d = \frac{3(1-\mu^2)pr^4}{16Et^3}\frac{f_{mn}^2}{\sqrt{\left(f_{mn}^2-f^2\right)^2+4f^2\xi^2}} \tag{1}$$

where μ and E are Poisson's ratio and Young's modulus of the diaphragm material, r stands for the radius of the diaphragm, t is the diaphragm thickness, p is the sound pressure, f is the frequency of acoustic wave, ξ is the damping coefficient, and f_{mn} is the mn order natural frequency of the diaphragm. The first-order natural frequency of diaphragm can be described as

$$f_{00} = \frac{10.17t}{r^2}\sqrt{\frac{E}{12\rho(1-\mu^2)}}. \tag{2}$$

Equation (1) suggests that using lower Young's modulus materials, at the same time, reducing the thickness-to-diameter ratio of diaphragm can improve obviously the sensitivity of FPI pressure sensors. Due to its preponderant physical properties such as low Young's modulus, non contraction after curing, flexible and light-reflecting, the 3M RITE-LOK UV-60 adhesive is selected to fabricate large area diaphragm for very low frequency acoustic sensing in this paper. The UV adhesive diaphragm fabrication process is schematically shown in Fig. 1.

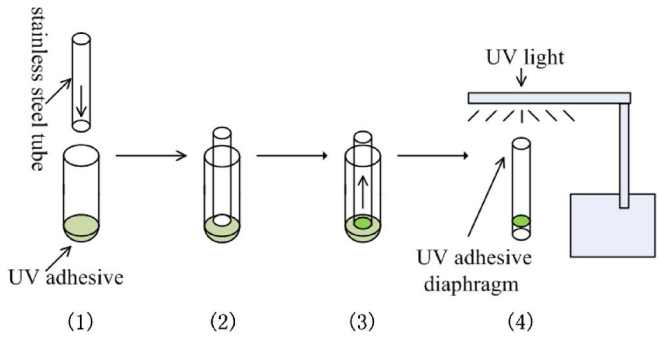

Fig. 1. Steps of fabrication UV adhesive diaphragm (1)–(4).

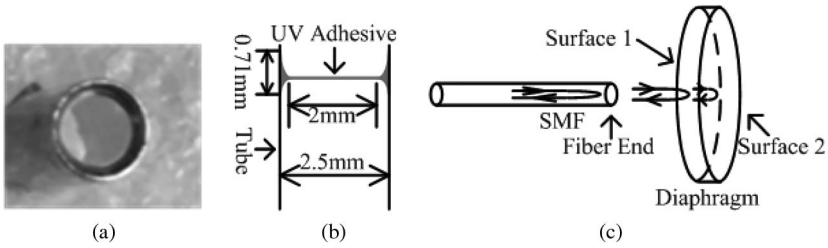

Fig. 2. (a) UV adhesive diaphragm. (b) Sectional view of UV adhesive diaphragm. (c) Schematic diagram of detecting thickness of diaphragm.

To fabricate the UV adhesive diaphragm, 5 ml 3M RIT-LOCK UV-60 adhesive solution is firstly prepared in the test tube, and then, a clearly stainless steel tube with 9 mm length, 1.25 mm inner radius, and 1.5 mm outer radius is inserted into the UV adhesive solution about 1 mm vertically. After about 40 s, the internal surface of stainless steel tube will adhere to UV adhesive solution uniformly. Next, pull out the stainless steel tube from UV adhesive solution slowly. Because of the surface wettability of stainless steel tube and surface tension of UV adhesive solution, a thin UV adhesive diaphragm will be formed and its edge will be fixed on the internal surface of stainless steel tube. For purpose of improving the stability of diaphragm, the UV adhesive diaphragm is exposed to the UV light continuously for 10 min. to solidify completely. At last, a diaphanous, smooth, stable and thin diaphragm is fabricated as shown in Fig. 2(a). It is a remarkable fact that the whole process is rather cost-effective and simple.

The thickness of UV adhesive diaphragm could be controlled by the depth of stainless steel tube in the UV adhesive and the speed of taking the stainless steel tube out from UV adhesive solution. Moreover, the thickness of diaphragm can be detected by calculating the free spectral range (FSR) from the interference spectrum of fiber-tip FPI as shown in Fig. 2(c). For a low-finesse FPI, the total reflected light intensity collected by the SMF from fiber end, surfaces 1 and surfaces 2 can be expressed by [20]

$$I = E_0^2 + E_1^2 + E_2^3 - 2E_0E_1\cos\left(\frac{4\pi}{\lambda}n_{\text{air}}d\right) + 2E_0E_2\cos\left[\frac{4\pi}{\lambda}(n_{\text{air}}d + n_{\text{UV}}t)\right] - 2E_1E_2\cos\left(\frac{4\pi}{\lambda}n_{\text{UV}}t\right) \tag{3}$$

where E_0, E_1, and E_2 are the amplitudes of three reflected waves; d is the length of FP cavity; t is the thickness of UV adhesive diaphragm; λ is the light wavelength; and n_{air} and n_{UV} are the refractive index of air and the UV adhesive diaphragm. Moreover, the interference spectrums of fiber-tip FPI with different thickness of UV adhesive diaphragm are shown in Fig. 3. Since the UV adhesive diaphragm is very thin, the modulation of the fringe envelope in Fig. 3 is regarded

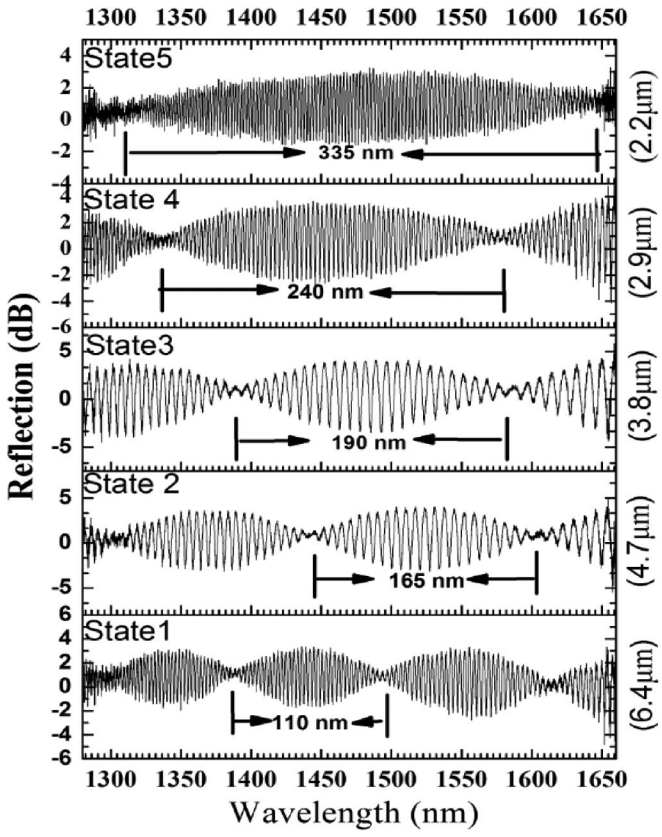

Fig. 3. Interference spectrum of fiber-tip FPI with different thickness of UV adhesive diaphragm.

as the result of the interference between surface 1 and surface 2. Therefore, the thickness of UV adhesive diaphragm can be expressed as

$$t = \frac{\lambda^2}{(2n_{\mathrm{UV}}\mathrm{FSR}_{\mathrm{env}})} \tag{4}$$

where $\mathrm{FSR}_{\mathrm{env}}$ is the spacing of fringe-envelope in Fig. 3 and they are 110 nm, 165 nm, 190 nm, 240 nm, and 335 nm from state 1 to 5, respectively. Moreover, n_{UV} is about 1.5. Based on (4), the corresponding diaphragm thickness from state 1 to 5 are about 6.4, 4.7, 3.8, 2.9, and 2.2 μm, respectively.

Considering the vibration of diaphragm as undamped vibration and $f \ll f_{00}$ in formula (1), the deformation of diaphragm will be irrelevant to the frequency of acoustic wave and can be expressed as

$$\Delta d = \frac{3(1-\mu^2)pr^4}{16Et^3}. \tag{5}$$

Therefore the maximum working frequency of the sensor should be considerably smaller than the resonant frequency of the diaphragm, but (5) and (2) suggest that the lower thickness-to-diameter ratio of diaphragm, the higher sensitivity, and the lower resonant frequency of FPI sensor head that can be obtained.

The Young's modulus, Poisson's ratio and density of 3M RIT-LOCK UV-60 adhesive are about 2.5 GPa, 0.4, and 850 kg/m^3, respectively. Calculated by (4) and (2), the theoretical sensitivity and resonant frequency of UV adhesive diaphragm with 1 mm radius and 6.4 μm thickness are 250 nm/pa and 5617 Hz respectively. What is noteworthy is that the diaphragm isn't

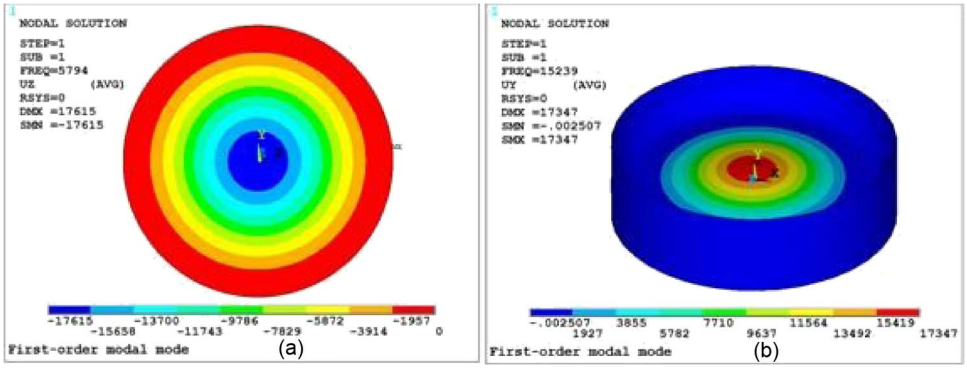

Fig. 4. First-order modal modes of flat and gradually increased UV adhesive diaphragm.

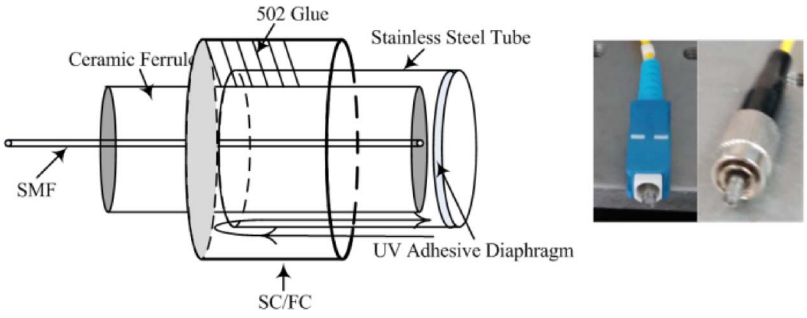

Fig. 5. Configuration of fiber acoustic sensor.

fabricated at outermost tip of stainless steel tube but inside the tube and the thickness of diaphragm edge is gradually increased as shown in Fig. 2(b), which can protect the diaphragm from outer damage in some degree. What's more, there is a relatively large contact area between the diaphragm and tube surface to ensure the diaphragm fixed on the tube firmly. The most important, it will improve the natural frequency of diaphragm for the effective thickness increasing. The simulation values of first-order natural frequency of flat and gradually increased diaphragm calculated by ANSYS are about 5794 and 15 239 HZ as show in Fig. 4. It means that the UV adhesive diaphragm with 1 mm radius and 6.4 μm thickness can be selected as sensing diaphragm to achieve a high sensitivity and a relative high resonant frequency at the same time.

To form an extrinsic FPI acoustic sensor, the ceramic ferrule of commercial SC or FC is inserted in the stainless steel tube that includes an UV adhesive diaphragm. Then the stainless steel tube is fixed on the SC or FC by the 502 glue, but the 502 glue did not seal the FP cavity leaving a space to balance the pressure difference between inside and outside of FP cavity as shown in Fig. 5. If ignoring the refection light of surfaces 2, the total refection light intensity in (2), which contains the acoustic signal traveling back along the SMF, can be expressed

$$I \approx E_0^2 + E_1^2 - 2E_0E_1\cos\left(\frac{4\pi}{\lambda}n_{\text{air}}d\right). \tag{6}$$

Therefore, the acoustic signal can be demodulated directly by the reflection light intensity changes when a narrowband laser whose wavelength at Q-point is incident into a FPI acoustic sensor [21].

3. Experiment Results and Discussion

In order to demonstrate the potential of UV adhesive diaphragm-based FPI as a highly sensitive acoustic sensor, a contrast experiment is employed as shown in Fig. 6. A tunable laser is used

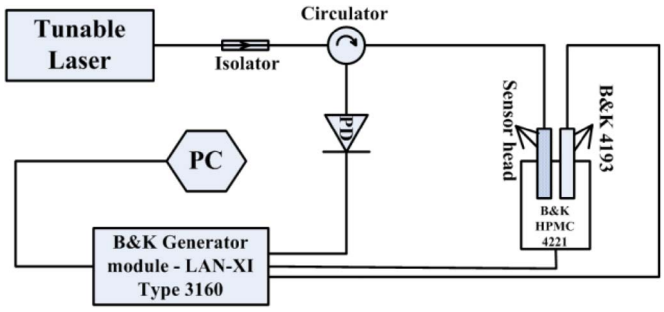

Fig. 6. Schematic diagram of experimental setup for acoustic pressure measurement.

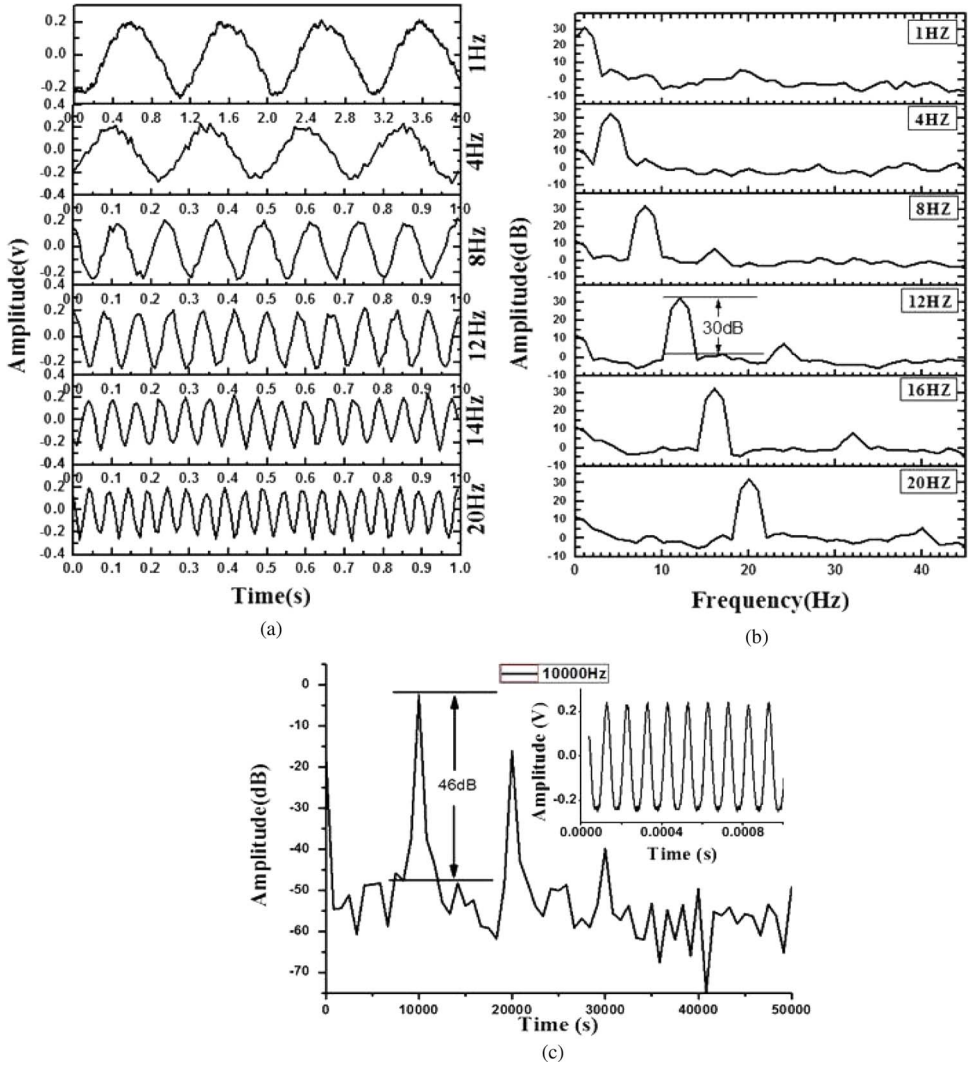

Fig. 7. (a) Outputs of the acoustic sensor from 1 to 20 Hz and (b) their corresponding frequency spectral after a FFT transformation. (c) Outputs of the acoustic sensor at 10 000 Hz and frequency spectral after a FFT transformation.

to keep FPI sensor head working at Q-point for maximizing the acoustic sensitivity [22]. The reflected light of the FPI sensor head through an optical circulator is detected by a photo detector (PD, New Focus 1623). The acoustic signal is generated by the B&K High Pressure Microphone Calibrator

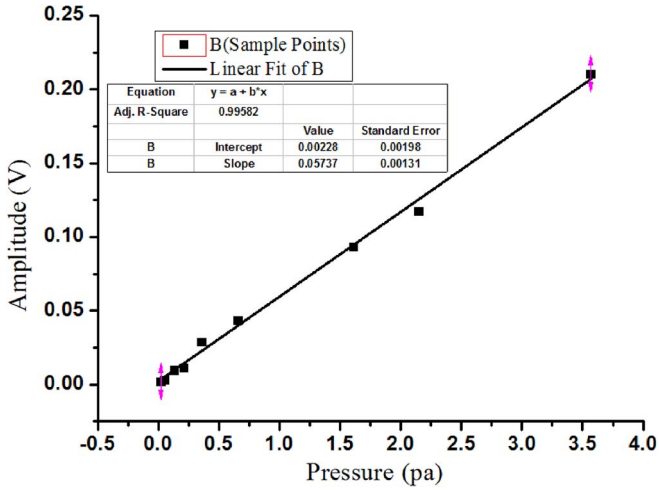

Fig. 8. Output signal of the proposed sensors for varying applied acoustic pressure levels at the frequency of 1000 Hz.

(HPMC) 4221 driven by B&K Generator module-LAN-XI Type 3160, which can worked as a sound source in the pressure field. The microphone of B&K 4193 with a sensitivity of 12.5 mV/Pa and a frequency response ranging from 0.07 Hz to 20 kHz is used for calibration and comparison with the FPI sensor head in the pressure field. They are both inserted into the HPMC 4421 and the achieved acoustic signals of which are transmitted to Type 3160. The combination of inputs and output channels makes Type 3160 one of the most versatile data acquisition modules available, while interchangeable front-panels give the flexibility to use a wide range of transducers. Moreover, this low-frequency calibration system is only applicable in the pressure field.

Fig. 7(a) and (b) show the time domain waveform detected by the FPI sensor head at the same pressure of 538.3 mPa from 1 to 20 Hz, as well as the corresponding frequency spectrum after FFT transform. From the experimental results, a stable signal-to-noise ratio (SNR) about 30 dB with a noise floor at 0 dB and a 2 Hz resolution can be observed ranging from 1 to 20 Hz respectively, and its noise-limited minimum detectable pressure is about 11.2 mPa/Hz$^{1/2}$. That means the very low frequency ranging from 1 to 20 Hz can be interrogated well by our proposed FPI acoustic sensor. The high frequency acoustic wave of 10 000 Hz is also detected by the acoustic sensor as shown in Fig. 7(c). When the applied acoustic pressure is 93.5 mPa, the proposed sensor shows a SNR of 46 dB with a noise floor at –48 dB and a resolution of 80 Hz, and the corresponding noise-limited minimum detectable pressure is 52.4 μPa/Hz$^{1/2}$. The noise-limited minimum detectable pressure of low frequency is much higher than that of high frequency for the high noise floor at low frequency. The highly low-frequency noise can be further reduced by enhancing the packaging technology to decrease the noise from low frequency vibration and temperature change caused by ambient environment [22]. The demodulation system also can be further improved by reducing the influence of power fluctuation and working point shift of acoustic sensors to increase the SNR [21], [23]. Moreover, the harmonics shown in Fig. 7(b) and (c) allow us to further identify the detected acoustic frequency [14].

Fig. 8 shows the output voltage signal of the proposed sensor when the acoustic pressure is increased from 21.4 mPa to 3.56 Pa by controlling the voltage of Calibrator 4221 at 1000 Hz. The result indicates the proposed sensor has a linear response with a linear correlation coefficient (R^2) of 0.99582 under given sound pressure levels. From the slope of the fitted curve, the sensitivity of FPI acoustic sensor can be achieved about 57.3 mV/Pa which is higher than that of B&K 4193.

The frequency response of the proposed FPI acoustic sensor from 1 Hz to 20 kHz is shown in Fig. 9. The acoustic pressures generated from B&K Calibrator 4221 at different frequencies are calibrated by the microphone of B&K 4193. A dominant resonance peak at approximately 18 kHz can be observed in Fig. 9, which is close to the simulation value about 15 239 Hz and

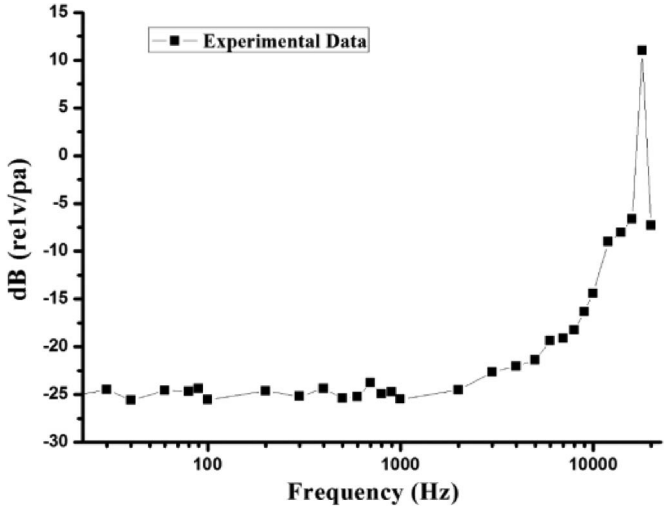

Fig. 9. Frequency response of proposed FPI acoustic sensor.

TABLE 1

Fabrication process and performance parameters of selected acoustic sensors in recent years

Diaphragm	Technology	Sensitivity	Resolution	Freq. Range	Ref.
Multilayer graphene	Chemical vapor deposition	13.15mv/pa	59.5μPa/Hz$^{1/2}$@10kHz	200Hz to 22kHz	[13]
Photonic-Crystal Silicon	Electro-mechanical model		33μPa/Hz$^{1/2}$@1-30kHz	1kHz to 30kHz	[18]
Center-Embossed silicon	Micromachining	18.6mv/pa		10Hz to 2 kHz	[11]
Large-area nanolayer silver	Electroless plating		14.5μPa/Hz$^{1/2}$ @4kHZ	400Hz to 8.5kHz	[24]
Adhesive diaphragm	Surface tension	57.3mv/pa	52.4μPa/Hz$^{1/2}$@10kHz; 11.2mPa/Hz$^{1/2}$@1-20Hz	1HZ to20kHz	Our scheme

suggests the gradually increased thickness of diaphragm edge can improve the natural frequency of diaphragm significantly. Because it is hard to measure the curvature of thickness change of diaphragm edge accurately, the resonance frequency of proposed fiber sensor is little different to the simulation value. The flat frequency response range is from 1 Hz to 2000 Hz with a small fluctuation about ±1.5 dB. That means the FPI acoustic sensor can be used for very-low-frequency acoustic sensing very well. In addition, the working frequency range of proposed acoustic sensor can be further extended by reducing the radius and increasing the thickness of UV adhesive diaphragm to improve the resonance frequency of sensing diaphragm.

As shown in Table 1, some kinds of diaphragms have been fabricated for fiber acoustic sensing and exhibit good performance in recent years, but the fabrication processes of them are costly and complex. In addition, they are insensitive to low-frequency acoustic wave, particularly for infrasound. The proposed FPI acoustic sensor has been demonstrated superior property of low-frequency acoustic sensing with high sensitivity and good infrasound response. Most importantly, the fabrication process of adhesive diaphragm is rather simple and low-cost, just curing UV adhesive after diaphragm formed by surface tension.

4. Conclusion

In summary, a novel UV adhesive diaphragm-base FPI fiber sensor for infrasound measurement has been proposed and experimentally demonstrated. The fabrication process of sensing

diaphragm is rather simple and low cost with no other chemical, except for UV adhesive. The acoustic detection has been performed at the frequencies in the range of 1 Hz to 20 kHz, and the sensor exhibits a flat frequency response ranging from 1 Hz to 2000 Hz with a small fluctuation about ±1.5 dB. The sensitivity and SNR of proposed sensor are 57.3 mV/Pa and 30 dB. The sensor exhibits a noise limited detectable pressure of 52.4 μPa/Hz$^{1/2}$ at 10 kHz and 11.2 mPa/Hz$^{1/2}$ ranging from 1 to 20 Hz. Such FPI fiber acoustic sensor can be applied as high sensitive and very-low-frequency acoustic sensor for earthquake sound detection.

References

[1] Y. Ishihara *et al.*, "Infrasound observations at Syowa Station, east antarctica: Implications for detecting the surface environmental variations in the polar regions," *Geosci. Frontiers*, 2015, vol. 6, no. 2, pp. 285–296, Mar. 2015.

[2] X. L. Pang, Y. Wang, Y. Ma, and X.-Y. Cheng, "Research on three-station location method for nuclear explosion infrasound detection," *Appl. Mech. Mater.*, vol. 727/728, pp. 651–655, Dec. 2015.

[3] F. Tanimola and D. Hill, "Distributed fibre optic sensors for pipeline protection," *J. Nat. Gas Sci. Eng.*, vol. 1, no. 4/5, pp. 134–143, Nov. 2009.

[4] G. V. Batanov, "Characteristics of etiology of immediate hypersensitivity in conditions of exposure to infrasound," *Radiats. Radioecol. Radioecol.*, vol. 35, no. 1, pp. 78–82, Jan./Feb. 1994.

[5] C. K. Kirkendall and A. Dandridge, "Overview of high performance fibre-optic sensing," *J. Phys. D, Appl. Phys.*, vol. 37, no. 18, pp. R197–R216, Sep. 2004.

[6] J. G. V. Teixeira, I. T. Leite, S. Silva, and O. Frazão, "Advanced fiber-optic acoustic sensors," *Photon. Sensors*, vol. 4, no. 3, pp. 198–208, Sep. 2014.

[7] C. Davis *et al.*, "Reduced length fibre bragg gratings for high frequency acoustic sensing," *Meas. Sci. Technol.*, vol. 25, no. 12, Oct. 2014, Art. ID 125105.

[8] M. A. Zumberge *et al.*, "An optical fiber infrasound sensor: A new lower limit on atmospheric pressure noise between 1 and 10 Hz," *J. Acoust. Soc. Amer.*, vol. 113, no. 5, pp. 2474–2479, May 2003.

[9] A. Abdallah, C. Z. Zhang, and Z. Zhong, "Acoustic pressure sensing with hollow-core photonic bandgap fibers," *Appl. Mech. Mater.*, vol. 738/739, pp. 61–64, Mar. 2015.

[10] B. Xu *et al.*, "Acoustic vibration sensor based on nonadiabatic tapered fibers," *Opt. Lett.*, vol. 37, no. 22, pp. 4768–4770, Nov. 2012.

[11] F. Wang *et al.*, "Extrinsic Fabry–Pérot underwater acoustic sensor based on micromachined center-embossed diaphragm," *J. Lightw. Technol.*, vol. 32, no. 23, pp. 4026–4034, Dec. 2014.

[12] Q. Wang and Q. Yu, "Polymer diaphragm based sensitive fiber optic Fabry–Pérot acoustic sensor," *Chin. Opt. Lett.*, vol. 8, no. 3, pp. 266–269, Mar. 2010.

[13] J. Ma *et al.*, "Fiber-optic Fabry–Pérot acoustic sensor with multilayer graphene diaphragm," *IEEE Photon. Technol. Lett.*, vol. 25, no. 10, pp. 932–935, May 2013.

[14] L. H. Chen, C. C. Chan, W. Yuan, S. K. Goh, and J. Sun, "High performance chitosan diaphragm-based fiber-optic acoustic sensor," *Sensors Actuators A, Phys.*, vol. 163, no. 1, pp. 42–47, Sep. 2010.

[15] F. Xu *et al.*, "High-sensitivity Fabry–Pérot interferometric pressure sensor based on a nanothick silver diaphragm," *Opt. Lett.*, vol. 37, no. 2, pp. 133–135, Jan. 2012.

[16] J. Teng, Y. Song, X. Jian, and M. Zhao, "Optical properties of polymer poly (phthalazinone ether sulfone ketone) film waveguide," *Chin. Opt. Lett.*, vol. 6, no. 1, pp. 74–75, Jan. 2008.

[17] W. Xiaodong *et al.*, "An ultra-sensitive optical MEMS sensor for partial discharge detection," *J. Micromech. Microeng.*, vol. 15, no. 3, pp. 521–527, Mar. 2005.

[18] W. Jo, O. C. Akkaya, O. Solgaard, and M. J. F. Digonnet, "Miniature fiber acoustic sensors using a photonic-crystal membrane," *Opt. Fiber Technol.*, vol. 19, no. 6, pp. 785–792, Dec. 2013.

[19] D. Giovanni, *Flat and Corrugated Diaphragm Design Handbook*. Boca Raton, FL, USA: CRC, 1982.

[20] C. Liao *et al.*, "Sub-micron silica diaphragm-based fiber-tip Fabry–Pérot interferometer for pressure measurement," *Opt. Lett.*, vol. 39, no. 10, pp. 2827–2830, May 2014.

[21] Q. Wang and Z. Ma, "Feedback-stabilized interrogation technique for optical Fabry–Pérot acoustic sensor using a tunable fiber laser," *Opt. Laser Technol.*, vol. 51, pp. 43–46, Oct. 2013.

[22] P. Hu *et al.*, "Study on high temperature Fabry–Pérot fiber acoustic sensor with temperature self-compensation," *Opt. Eng.*, vol. 54, no. 9, Sep. 2015, Art. ID 097104.

[23] S. N. Wang, M. Y. Zhang, Y. H. Cao, and L.-J. Chen, "A micro-machined optical fiber acoustic sensor based on Fabry–Pérot interferometer," in *Proc. ICOM*, 2013, pp. 167–169.

[24] F. Xu *et al.*, "Fiber-optic acoustic pressure sensor based on large-area nanolayer silver diaghragm," *Opt. Lett.*, vol. 39, no. 10, pp. 2838–2840, May 2014.